Dynamics of electron-emission currents in plasmonic gaps induced by strong fields

Garikoitz Aguirregabiria, Dana-Codruta Marinica, Markus Ludwig, Daniele Brida, Alfred Leitenstorfer, Javier Aizpurua, Andrei Borisov

Journal Name

ARTICLE TYPE

Cite this: DOI: 10.1039/xxxxxxxxxx

Dynamics of electron-emission currents in plasmonic gaps induced by strong fields†

Garikoitz Aguirregabiria,[a,b] Dana-Codruta Marinica,[c] Markus Ludwig,[d] Daniele Brida,[d,e] Alfred Leitenstorfer,[d] Javier Aizpurua*[a,b] and Andrey G. Borisov,*[c]

Received Date
Accepted Date

DOI: 10.1039/xxxxxxxxxx

www.rsc.org/journalname

The dynamics of ultrafast electron currents triggered by femtosecond laser pulse irradiation of narrow gaps of plasmonic dimer is studied using quantum mechanical time-dependent density functional theory. The electrons are injected into the gap by the optical field emission from the surfaces of metal nanoparticles across the junction. Further evolution of the electron currents in the gap is governed by the local enhanced electric fields. The combination of TDDFT and classical modelling of the electron trajectories allows us to study the quiver motion of the electrons in the gap region in dependence the carrier envelope phase of the incident pulse. In particular, we demonstrate the role of the quiver motion in establishing the CEP-sensitive net electric transport between nanoparticles.

Electron emission from metallic surfaces is a physical process which exploits the exchange of energy between incident photons and outgoing electrons[1,2]. The current trends in nanotechnology are able to design complex morphologies of metallic nanostructures which can act as effective optical nanoantennas trapping and enhancing light of specific wavelengths in their proximity[3–5]. This is achieved by means of the collective excitation of the electronic charge density at the interfaces of the metallic nanostructures, so-called surface plasmons[6,7]. Plasmonic nanoparticles are thus a very appealing structure for the generation of strong-field emitted electrons due to the electric-field enhancement and localization produced near the particles surface[8–15]. Among others, metallic tips have been commonly used in the generation of photoemitted electrons, for instance in the guns of electron microscopes[16].

More recently, the use of plasmonic gaps, constituted by the junction of a metal-insulator-metal interface have been shown to host very intense bonding-gap plasmons which produce electromagnetic hot spots commonly exploited in surface-enhanced spectroscopy[17–22]. The plasmonic gap has also been the object of intense research regarding the interplay between optical and transport properties, as the two metallic particles forming the gap can be externally biased, and the current across the gap can thus be accessed while illuminating the structure with light[22–27]. Last, but not least, the ability to shape light into ultra-short single-cycle pulses with varying carrier envelope phase (CEP) provides an additional degree of control on the photoelectrons emitted[9,13,24]. When those electrons are emitted in a plasmonic gap as a result of the incidence of an ultra-short pulse, a complex dynamical behaviour of the electrons can be foreseen which depend on the particular conditions of the emission, such as energy of the photons, duration of the pulse, local field enhancement, or separation of the gap[24]. Differently from a metallic tip, characterized by the electron emission into the free-space, plasmonic gap offers a possibility of achieving electron transport between nanoparticles controlled at the optical cycle timescale thus granting mutual coherence between radiation and electron current. A theoretical scheme capable of tracing the dynamics of these ultra-short electron bursts in plasmonic gaps can be extremely useful when it comes to design and control the optoelectronic properties of ultrafast electron currents.

This discussion precisely addresses the challenge of describing the complex dynamics of photoemitted currents in plasmonic gaps under ultra-short illumination. A simple model of the structure will help to provide an understanding of the interplay between the carrier envelope phase of a single pulse and the motion of the electron bursts in the gap. We describe our model system, the methodological approach to the dynamics of the electrons, and the results in the following sections.

[a] Centro de Física de Materiales CSIC-UPV/EHU, Paseo Manuel de Lardizabal 5, 20018, Donostia-San Sebastián, Spain. E-mail: aizpurua@ehu.eus
[b] Donostia International Physics Center, Paseo Manuel de Lardizabal 5, 20018, Donostia-San Sebastián, Spain.
[c] Institut des Sciences Moléculaires d'Orsay - UMR 8214, CNRS-Université Paris Sud, Batiment 351, 91405 Orsay Cedex, France. E-mail: andrei.borissov@u-psud.fr
[d] Department of Physics and Center for Applied Photonics, University of Konstanz, D-78457 Konstanz, Germany.
[e] Physics & Materials Science Research Unit, University of Luxembourg, 162a Avenue de la Faïencerie, L-1511, Luxembourg.

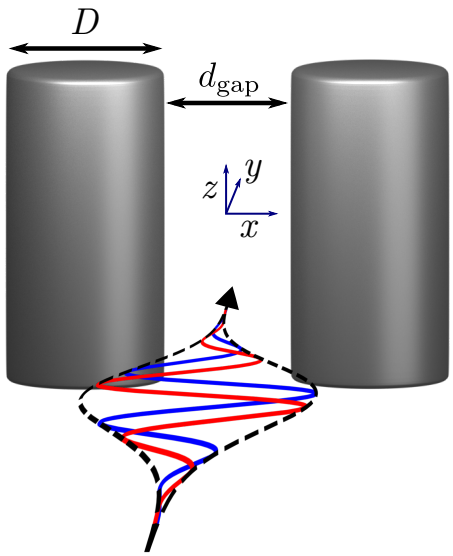

Fig. 1 Dimer of gold cylinders of diameter $D = 10$ nm and separated by a gap of $d_{\mathrm{gap}} = 3$ nm. The dimer is excited by a Gaussian laser pulse containing only one optical cycle. The Carrier Envelope Phase, ϕ, of the illumination is progressively modified in order to study the dynamics of the strong-field emitted electrons in the gap (blue line $\phi = 0$, red line $\phi = \pi/2$).

1 Plasmonic system

As a prototype of a plasmonic gap system we consider a dimer of parallel gold cylinders of diameter $D = 10$ nm as sketched in Fig. 1. The identical cylinders are infinite along the z-axis, and the distance between the two nanoparticle surfaces at the closest point is $d_{\mathrm{gap}} = 3$ nm. This structure is illuminated by a femtosecond (fs) Gaussian pulse $E(t)$ polarized along the x-axis passing through the centers of the cylinders. The duration of the pulse is roughly one optical period:

$$E(t) = \tilde{E}\cos(\omega t + \phi)e^{-t^2/\tau^2} \ , \tag{1}$$

where the amplitude of the electric field is $\tilde{E} = 3.7$ V/nm, ω is the carrier frequency, ϕ is the CEP and $\tau = (2\pi/\omega)/\sqrt{2\log(2)}$ is the duration of the pulse. Figure 1 shows two of the pulse CEPs used in the calculation: in blue $\phi = 0$ and in red $\phi = \pi/2$. We use the carrier frequencies ω in the near-infrared, thus far from the Bonding Dipolar Plasmon resonance of the dimer at Ω_p [25,28]. With present choice of the model for the electronic structure of gold cyliders discussed below, $\Omega_p = 5.5$ eV. The off-resonance excitation of the system allows the time-dynamics of the local fields in the gap close to that of the incident pulse (sub-cycle). Since the local field in the gap triggers the electron transport across the junction, it is expected that the net electronic transport will be sensitive to the CEP of the external pulse. This is while for the resonant excitation the dynamics of the field in the junction would be determined by the damping rate of the corresponding plasmon mode. As a result, except for extremely broad plasmon resonance, the local ac field in the gap would generally persist for long times after the end of the external transient. In such a situation, the averaging by many-cycle oscillations would lead to almost zero net current across the junction and very low sensitivity to the CEP of the incident pulse.

Under these illumination conditions, with the corresponding field enhancement in the gap, and the range of frequencies used, the Keldish parameter [29] (γ) obtained in this work is in the range of $\gamma \approx 0.48 - 1.90$, which is usually considered as optical-field emission regime [2,8,30,31].

2 Methodology

To treat the electron dynamics of the system under strong-field illumination we use a real time Time-Dependent Density Functional Theory (TDDFT) based on the Kohn-Sham (KS) scheme [32–34]. The Au cylinders are described with the so-called Stabilized Jellium Model (SJM) [35]. Within the SJM, the valence electrons are treated explicitly, while the atomic cores are represented as a positive background charge density

$$n^+ = \left(\frac{4\pi}{3}r_s^3\right)^{-1} \ , \tag{2}$$

where r_s is the Wigner-Seitz radius (here $r_s = 3.02\ a_0$, $1\ a_0 = 0.053$ nm). An attractive pseudopotential (V_{st} see below) is used so that the empirical work function of Au [36] $\Phi = 5.5$ eV is retrieved with the TDDFT calculations. Even though the use of the SJM neglects atomistic details and effects linked with localized d-electron bands, it allows to trace the dynamics of valence electrons in the metal, which are involved in the screening, photoemission, strong-field ionization, and transport properties in the plasmonic dimer. The jellium model of metal nanoparticles has been successfully used in the context of plasmonics allowing the theoretical prediction of quantum effects later confirmed experimentally [23,37,38] and TDDFT studies of strong-field emission from metal nanotips [39].

The time evolution of the KS orbitals is obtained from the 2D KS coupled equations (all equations are written in atomic units, a.u., unless otherwise indicated):

$$\left[-\frac{1}{2}\nabla^2 + V_{\mathrm{eff}}[n](x,y,t)\right]\Psi_k(x,y,t) = i\frac{\partial}{\partial t}\Psi_k(x,y,t) \ , \tag{3}$$

where Ψ_k are the KS orbitals, $\nabla = \hat{x}\frac{\partial}{\partial x} + \hat{y}\frac{\partial}{\partial y}$ and $V_{\mathrm{eff}}[n](x,y,t)$ is the effective KS potential given by:

$$\begin{aligned} V_{\mathrm{eff}}[n](x,y,t) =& V_{\mathrm{H}}[n](x,y,t) + V_{\mathrm{xc}}[n](x,y,t) \\ &+ V_{\mathrm{st}}(x,y) + V_{\mathrm{ext}}(x,t) \ . \end{aligned} \tag{4}$$

The Hartree potential, $V_{\mathrm{H}}[n](x,y,t)$, accounts for the interaction between a KS orbital and the charge density of the system. Due to the subwavelength scale of the relevant dimensions of the cylindrical dimer, the non-retarded approximation is considered in the calculations. The exchange-correlation potential, $V_{\mathrm{xc}}[n](x,y,t)$, effectively incorporates the exchange and correlation effects of the many-electron interacting system. Here we use the functional of O. Gunnarsson and B. I. Lundqvist [40] within the Adiabatic Local Density Approximation (ALDA) [34,41]. The stabilizing potential, $V_{\mathrm{st}}(x,y,t)$, corresponds to an attractive constant potential in the region of space filled by the nanoparticles, allowing to obtain the correct work function of gold as already discussed above. Finally, $V_{\mathrm{ext}}(x,t) = -xE(t)$ is the interaction potential between an electron

and the external electromagnetic field.

A combination of the Fourier-Grid Hamiltonian wavefunction representation[42–45] and the Split-Operator technique[43,46,47] is used to solve Eq. (3) by short time-step propagation. The initial conditions are $\Psi_k(x,y,t=0)=\Psi_k^0(x,y)$, where Ψ_k^0 correspond to the ground state KS orbitals retrieved from self-consistent Density Functional Theory (DFT)[48] calculation of the system in the absence of the external electromagnetic field.

The time-dependent electronic density and electron current density, $n(x,y,t)$ and $\vec{j}(x,y,t)$ respectively, are computed at each time step as follows:

$$n(x,y,t)=2\sum_{k\in occ}\chi_k\left|\Psi_k(x,y,t)\right|^2, \tag{5}$$

$$\vec{j}(x,y,t)=2\sum_{k\in occ}\chi_k\,\mathscr{I}\Updownarrow\left[\Psi_k^*(x,y,t)\;\hat{\mathbf{p}}\;\Psi_k(x,y,t)\right], \tag{6}$$

where $\hat{\mathbf{p}}=-i\vec{\nabla}$, the sum runs over all the occupied KS orbitals, the factor 2 accounts for the spin degeneracy, and $\chi_k=\frac{1}{\pi}\sqrt{2(E_F-E_i)}$ accounts for the number of electronic states associated to the z-motion. E_F stands for the Fermi level of the nanostructures and E_k for the ground-state energy of the orbital k.

3 Results

To study the dynamics of strong-field emitted electrons in the gap, we illuminate the system with the field transient given by Eq. (1) mimicking a single-cycle optical pulse, and at each time step we compute the electron current across the mid-plane of the gap,

$$J(x=0,t)=\int_{-\infty}^{\infty}\hat{e}_x\vec{j}(x=0,y,t)dy, \tag{7}$$

where $\hat{e}_x$ is the unit-length vector along x-axis.

Figure 2 shows the result of such analysis for the case of a pulse carrier frequency $\omega=0.67$ eV, where the electric field at the centre of the gap ($x=y=0$), $E_{\rm gap}$, is plotted in blue and the current density across the mid-plane of the gap, $J(x=0,t)$, is plotted in red. Note that $E_{\rm gap}$ comprises both: the electric field of the incident pulse and the induced electric field owing to the polarisation of nanowires. At the initial interval of time, $t<0$ fs, the electric field in the gap is not strong enough to produce a significant electron emission current. However, the central peak of the pulse at $t=0$ fs produces the emission of electrons from the surface of the cylinders on the right hand side in Fig. 1 and therefore a negative electronic current is observed at $t\approx 1$ fs. Around $t\approx 1.5$ fs, the field in the gap changes polarity and a second smaller current density peak can be observed, which flows in the opposite direction to the main one. This weaker current density is formed from two contributions, one coming from the electrons emitted from the cylinder situated on the left hand side in Fig. 1 and, as we will show below, a second contribution originated from electrons which were emitted from the right cylinder but did not reach the opposite nanoparticle before $E_{\rm gap}$ have changed polarity, thus inducing electron quiver motion.

Integrating in time the current in Eq. (7), one can obtain the number of electrons transferred across the gap. The analysis of

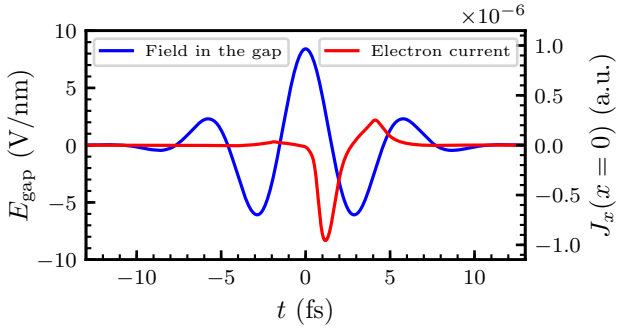

Fig. 2 TDDFT results for the dimer is illuminated by a pulse of frequency $\omega=0.67$ eV and CEP $\phi=0$. Blue line: electric field at the centre of the gap $E_{\rm gap}$. Red line: electron current across the mid-plane of the gap ($J(x=0,t)$).

the net electron transport as a function of CEP is shown in Fig. 3 for different carrier frequencies of the incident pulse. We first focus our attention on the smallest frequencies, $\omega=0.32$ eV (solid yellow line) and $\omega=0.48$ eV (solid pink line). For these frequencies, the results in Figure 3 show a behaviour consistent with direct propagation of emitted electrons across the junction with now quiver effect[10,12]: for a CEP $\phi=\pi/2$ or $\phi=3\pi/2$, the local field in the gap, $E_{\rm gap}$, is antisymmetric (sine-like) with respect to the center of the Gaussian envelope and thus, the field shows two identical peaks of opposite polarity (see red line in the sketch of Fig. 1). In such situation, the amount of electrons transferred in both directions is equal, compensates each other, and the net transport is zero. The maximum electron transfer occurs for $\phi=0$ or $\phi=\pi$. The incident electromagnetic pulse in this case has symmetric electric field profile, with main positive or negative peak of the field centered at $t=0$ (see Fig. 2). Because the optical-field emission process is highly non-linear 2012,Hommelhoff2018, the electron current in the junction is dominated by the ultra-short burst of electrons emitted at the half-period with strongest field as nicely seen in Fig. 2. Under an assumption that all electrons arrive to the opposite surface, the $\phi=0$ or $\phi=\pi$ correspond to the maximum number of electrons transferred in positive ($\phi=\pi$) or negative ($\phi=0$) direction.

However, when the illumination frequency is increased, the CEP at which the maximum electron transfer is produced shifts away from the expected $\phi=0$ and $\phi=\pi$ values. In contrast to single nanoparticles where the evanescent near-field decays rapidly as the distance to the nanoparticle's surface is increased and the quiver motion might be quenched[10], the field in small plasmonic gaps is almost constant across the full distance separating the nanoparticles, therefore, the quiver motion of the electrons emitted needs to be considered in a gap. This quiver motion of the electrons in the gap is responsible for the shift of the value of the CEP to achieve the maximum net electron current shown in Fig. 3, as we analyse below.

Classical analysis

We employ a classical Simpleman's model (SMM) to study the quiver motion of the photoemitted electrons in plasmonic gap, and the role it plays in electron transfer between the nanopar-

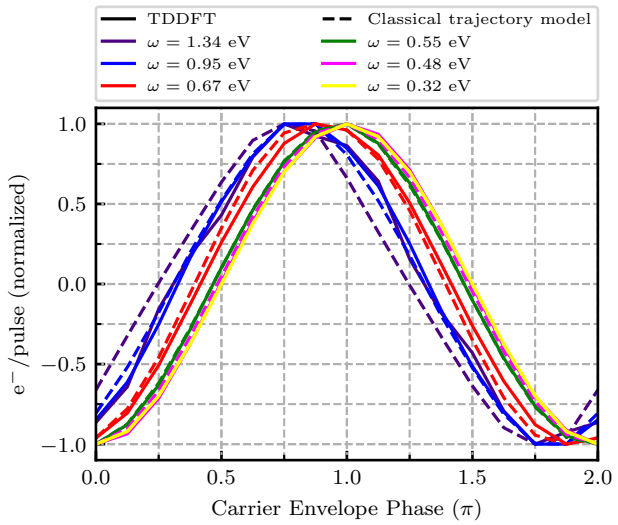

Fig. 3 Normalized electron transfer as a function of the illumination CEP ϕ. Different colors are used for the number of electrons transferred per pulse as obtained with different carrier frequencies. The color code is explained in the insert at the top of the figure. Solid lines: results of the TDDFT calculations; dashed lines: results obtained using the Simpleman's model for electron emission and transport. The quiver amplitude associated to each of the frequencies ($\omega = 0.32$ eV, 0.48 eV, 0.55 eV, 0.67 eV, 0.95 eV, 1.34 eV) is $X_q = 6.33$ nm, 2.82 nm, 2.12 nm, 1.42 nm, 0.72 nm and 0.37 respectively.

ticles. The SMM has been first developed for the optical field electron emission from atomic species[49–51], and later successfully applied to electron emission from surfaces of metallic tips[30,31,39]. To qualitatively capture the main physics, while keeping the analysis of the results simple, we neglect the 2D aspect of the problem and only consider the electron motion along the x-axis. The optical field electron emission is approached as a two step process. First, we use the field in the gap $E_{\rm gap}$ obtained from the TDDFT calculations to compute the instantaneous Fowler-Nordheim tunneling current[52], $J_{\rm FN}$, at each time step within the pulse,

$$J_{\rm FN} \propto -E_{gap}(t_e)\left|E_{\rm gap}(t_e)\right| \exp\left[\frac{b\Phi^{\frac{3}{2}}}{\left|E_{\rm gap}(t_e)\right|}\right] , \qquad (8)$$

where $b = 6.83$ V/(nm eV$^{3/2}$), $\Phi = 5.5$ eV is the work function of gold, and $E_{\rm gap}(t_e)$ is the electric field in the gap at the time instant of emission defined as t_e. The second step consists in calculating the classical trajectory on the x-axis of an electron emitted at time t_e and subjected to the time dependent electric field $E_{\rm gap}$ (assuming that $E_{\rm gap}$ is homogeneous in the gap region):

$$\dot{v}_x = -E_{\rm gap} \ . \qquad (9)$$

where $e = m_e = 1$.

The initial conditions $v_x(t_e) = 0$ correspond to a tunneling electron emerging from the potential barrier at the metal/vacuum interface into the classically allowed region in the gap. Using the relationship between the electric field and the vector potential (A), $E = -dA/dt$, the velocity of the classical electron at any time $t > t_e$ is:

$$v_x(t) = A_{\rm gap}(t) - A_{\rm gap}(t_e) \ . \qquad (10)$$

This trajectory is computed until the electron reaches the surface of one of the two cylinders. If the electron crosses the gap, the trajectory is considered for the calculation of the net charge transfer assuming that it contributes with a weight given by Eq. (8). The trajectory is discarded if ,because of the quiver motion, it returns back to the initial nanoparticle.

Analysing Eq. (10), a third scenario is possible. If an electron is emitted at a time t_e such that $E_{\rm gap}$ is a local maximum, the associated vector potential is $A_{\rm gap}(t_e) = 0$. Furthermore, the finite duration of the illumination transient ensures that $A_{\rm gap}(t \to \infty) = 0$. Therefore, electrons emitted within the condition $A_{\rm gap}(t_e) = 0$, might end up in the middle of the gap with velocity $v_x(t \to \infty) = 0$. We will call the corresponding trajectories as "trapped" trajectories.

The electron transfer across the plasmonic gap calculated with SMM as function of the CEP and frequency of the incident pulse is shown with dashed lines in Fig. 3. The agreement with the TDDFT calculations (solid lines) is remarkable. The Simpleman's model allows to identify the quiver amplitude X_q as a key parameter controlling the electron transfer. The quiver amplitude, X_q, is the amplitude of the oscillatory movement of an electron in a homogeneous harmonic electric field $E(t) = E_0 \cos(\omega t)$ of frequency ω and amplitude strength E_0:

$$X_q = \frac{E_0}{\omega^2}. \qquad (11)$$

Using for E_0 the maximum of the total field generated in the gap, $E = [E_{\rm gap}]_{\rm max} \approx 8.45$ V/nm, the frequencies $\omega = 0.32$ eV, 0.48 eV, 0.55 eV, 0.67 eV, 0.95 eV and 1.34 eV are characterized by the corresponding quiver amplitudes $X_q = 6.33$ nm, 2.82 nm, 2.12 nm, 1.42 nm, 0.72 nm and 0.37 nm respectively. Then, as follows from the results presented in Fig. 3, the maximum electric transport is produced at CEP $\phi = 0$ or $\phi = \pi$ only for the cases where $X_q \gtrsim d_{\rm gap}$.

Figure 4 shows the electric field in the gap (left line plot in each panel) and the color map formed by classical electron trajectories (right of each panel) for three different carrier frequencies selected in such a way that the respective quiver amplitudes belong to the two different regimes, i.e., $X_q \gtrsim d_{\rm gap}$ and $X_q < d_{\rm gap}$. In the three cases the CEP is considered to be $\phi = \pi$. The velocity of the electron in each trajectory is colour-coded. The positive velocity ($v_x > 0$) is marked in red and the negative velocity ($v_x < 0$) is marked in blue. The width of each line is linked with the tunneling current in Eq. (8), which indicates that a larger amount of charge is moving along wider lines. In the three examples quiver motion is observed depending on the moment t_e when the electrons are emitted. In Fig. 4a, $X_q = 2.82$ nm and thus, most of the electron trajectories reach the opposite nanoparticle before the ballistic motion is inverted. In particular it can be observed how almost all the trajectories involving a large number of emitted electrons (wider lines) directly reach the opposite nanoparticle, corroborating that the maximum net electron transfer occurs for $\phi = \pi$ (see pink line in Fig. 3)

Figures 4b,c show the situation where $X_q < d_{\rm gap}$. In both cases the quiver motion is more obvious and relevant as X_q decreases. Increasing number of trajectories are reflected back because the

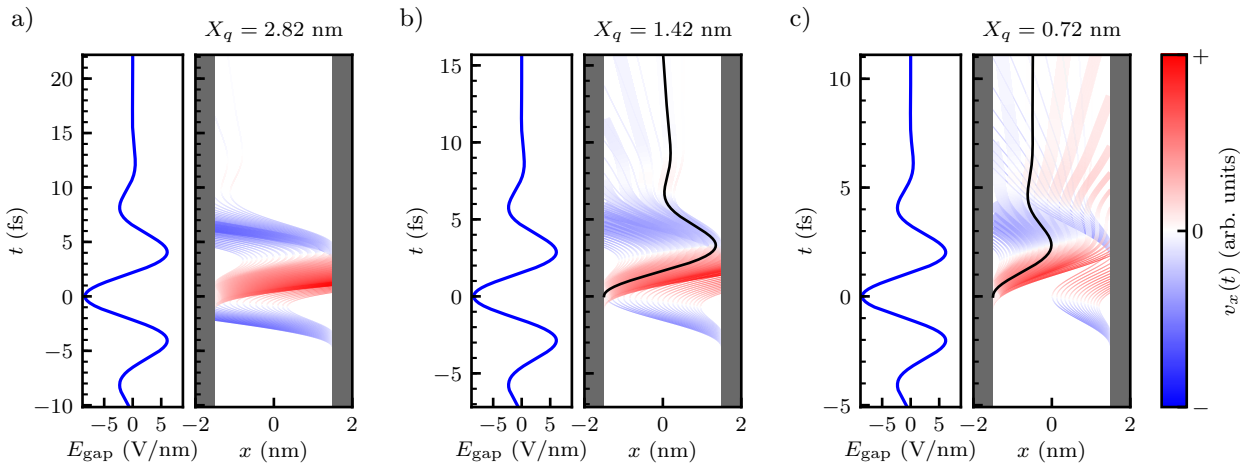

Fig. 4 Classical trajectories obtained using the Simpleman's model for carrier frequencies of the incident pulse a) $\omega = 0.48$ eV, b) $\omega = 0.67$ eV and c) $\omega = 0.95$ eV. In all cases the CEP $\phi = \pi$. The electric field at the centre of the gap, $E_{\rm gap}$, (horizontal axis) as a function of time (vertical axis) is shown at the left of each panel. The classical trajectories of electrons emitted along the x-axis are shown to the right of each panel. The position x in shown in the horizontal axis and the time in the vertical axis. The x-component of the velocity of the electrons in each trajectory is colour-coded with positive velocity in read and negative in blue. The velocity in each panel is normalized to the range $[-v_x^{\rm max}, v_x^{\rm max}]$. The weight of each trajectory as given by Eq. (8) is represented by the width of the corresponding trajectory line. Wider lines imply a larger weight and thus a larger amount of charge moving along such trajectory. The black lines in a) and b) mark two examples of "trapped" trajectories.

polarity of the field has changed before they reach the opposite side of the gap. It is particularly relevant that in these two cases many of the trajectories involving a large number of emitted electrons (wide lines) are not able to cross the gap and thus the maximum electron transfer no longer occurs for the incident pulse with CEP $\phi = \pi$ which is the value displayed in this figure. This effect is consistent with the situation observed for larger illumination frequencies displayed with blue and red lines in Fig. 3. The black lines in Figs. 4b,c follow two examples of "trapped" trajectories where, as already mentioned, the final velocity is $v_x \approx 0$. The electrons moving along "trapped" trajectories are thus stopped in the middle of the gap upon the termination of the electromagnetic pulse. In practice, these electrons will be absorbed by the substrate or deviated by the stray fields without contributing to the coherent charge transport. As follows from the discussion above, the classical SMM analysis is a powerful and intuitive tool to trace the dynamics of ultrafast electron currents in plasmonic gaps driven by light.

4 Discussion and conclusion

Using a combination of quantum calculations (TDDFT) and classical modelling (Simpleman's model) we have been able to address the complex dynamics of strong-field emission currents in plasmonic gaps. In contrast with the reported results using metallic tips [10,12], we observed that the homogeneous field distribution characteristic of small plasmonic gaps produces a situation where the quiver motion of electrons has a substantial impact on the electron current. The ratio between the electron quiver amplitude, X_q, and the gap distance separating the nanoparticles, $d_{\rm gap}$, is a key parameter to establish the absolute CEP which produces the maximum electron transport between nanoparticles. These results reveal the importance of the CEP of an incident pulse to control the mutual coherence between electron and photon dynamics in specific metallic junctions.

Conflicts of interest

There are no conflicts of interest to declare.

Acknowledgements

G.A. acknowledges project PI2017-30 of the Departamento de Educación, Política Lingüística y Cultura of the Basque government and, G.A. and J.A. acknowledge funding from project FIS2016-80174-P of the Ministry of Economy, Industry and Competitiveness MINEICO.

Notes and references

1 P. Dombi, S. E. Irvine, P. Rácz, M. Lenner, N. Kroó, G. Farkas, A. Mitrofanov, A. Baltuška, T. Fuji, F. Krausz and A. Y. Elezzabi, Optics Express, 2010, **18**, 24206–24212.
2 S. V. Yalunin, M. Gulde and C. Ropers, Physical Review B, 2011, **84**, 195426.
3 J. Aizpurua, G. W. Bryant, L. J. Richter, F. G. De Abajo, B. K. Kelley and T. Mallouk, Physical Review B, 2005, **71**, 235420.
4 M. Pelton, J. Aizpurua and G. Bryant, Laser & Photonics Reviews, 2008, **2**, 136–159.
5 L. Novotny and N. Van Hulst, Nature Photonics, 2011, **5**, 83–90.
6 S. A. Maier, Plasmonics: fundamentals and applications, Springer Science & Business Media, 2007.
7 L. Novotny and B. Hecht, Principles of nano-optics, Cambridge university press, 2012.
8 R. Bormann, M. Gulde, A. Weismann, S. V. Yalunin and C. Ropers, Physical Review Letters, 2010, **105**, 147601.
9 M. Krüger, M. Schenk and P. Hommelhoff, Nature, 2011, **475**, 78.
10 G. Herink, D. R. Solli, M. Gulde and C. Ropers, Nature, 2012, **483**, 190.

11 D. J. Park, B. Piglosiewicz, S. Schmidt, H. Kollmann, M. Mascheck and C. Lienau, Physical Review Letters, 2012, **109**, 244803.

12 P. Dombi, A. Hörl, P. Rácz, I. Márton, A. Trügler, J. R. Krenn and U. Hohenester, Nano Letters, 2013, **13**, 674–678.

13 B. Piglosiewicz, S. Schmidt, D. J. Park, J. Vogelsang, P. Groß, C. Manzoni, P. Farinello, G. Cerullo and C. Lienau, Nature Photonics, 2014, **8**, 37.

14 M. Lehr, B. Foerster, M. Schmitt, K. Krüger, C. Sönnichsen, G. Schönhense and H.-J. Elmers, Nano Letters, 2017, **17**, 6606–6612.

15 W. P. Putnam, R. G. Hobbs, P. D. Keathley, K. K. Berggren and F. X. Kärtner, Nature Physics, 2017, **13**, 335.

16 A. V. Crewe, D. N. Eggenberger, J. Wall and L. M. Welter, Review of Scientific Instruments, 1968, **39**, 576–583.

17 P. Nordlander, C. Oubre, E. Prodan, K. Li and M. I. Stockman, Nano Letters, 2004, **4**, 899–903.

18 P. Mühlschlegel, H.-J. Eisler, O. J. F. Martin, B. Hecht and D. W. Pohl, Science, 2005, **308**, 1607–1609.

19 I. Romero, J. Aizpurua, G. W. Bryant and F. J. G. De Abajo, Optics Express, 2006, **14**, 9988–9999.

20 H. Xu, E. J. Bjerneld, M. Käll and L. Börjesson, Physical Review Letters, 1999, **83**, 4357.

21 S. S. Acimovic, M. P. Kreuzer, M. U. González and R. Quidant, ACS Nano, 2009, **3**, 1231–1237.

22 M. Liao, S. Jiang, C. Hu, R. Zhang, Y. Kuang, J. Zhu, Y. Zhang and Z. Dong, Nano Letters, 2016, **16**, 4040–4046.

23 K. J. Savage, M. M. Hawkeye, R. Esteban, A. G. Borisov, J. Aizpurua and J. J. Baumberg, Nature, 2012, **491**, 574–577.

24 T. Rybka, M. Ludwig, M. F. Schmalz, V. Knittel, D. Brida and A. Leitenstorfer, Nature Photonics, 2016, **10**, 667.

25 D. C. Marinica, M. Zapata, P. Nordlander, A. K. Kazansky, P. M. Echenique, J. Aizpurua and A. G. Borisov, Science Advances, 2015, **1**, e1501095.

26 D. R. Ward, F. Hüser, F. Pauly, J. C. Cuevas and D. Natelson, Nature nanotechnology, 2010, **5**, 732.

27 T. L. Cocker, V. Jelic, M. Gupta, S. J. Molesky, J. A. J. Burgess, G. De Los Reyes, L. V. Titova, Y. Y. Tsui, M. R. Freeman and F. A. Hegmann, Nature Photonics, 2013, **7**, 620.

28 G. Aguirregabiria, D. C. Marinica, R. Esteban, A. K. Kazansky, J. Aizpurua and A. G. Borisov, Physical Review B, 2018, **97**, 115430.

29 L. Keldysh et al., Sov. Phys. JETP, 1965, **20**, 1307–1314.

30 M. Krüger, M. Schenk, M. Förster and P. Hommelhoff, Journal of Physics B: Atomic, Molecular and Optical Physics, 2012, **45**, 074006.

31 M. Krüger, C. Lemell, G. Wachter, J. Burgdörfer and P. Hommelhoff, Journal of Physics B: Atomic, Molecular and Optical Physics, 2018, **51**, 172001.

32 W. Kohn and L. J. Sham, Physical Review, 1965, **140**, A1133.

33 E. Runge and E. K. U. Gross, Physical Review Letters, 1984, **52**, 997.

34 M. A. Marques and E. Gross, Annual Review of Physical Chemistry, 2004, **55**, 427–455.

35 J. P. Perdew, H. Q. Tran and E. D. Smith, Phys. Rev. B, 1990, **42**, 11627–11636.

36 E. V. Chulkov, V. M. Silkin and P. M. Echenique, Surface Science, 1999, **437**, 330–352.

37 R. Esteban, A. G. Borisov, P. Nordlander and J. Aizpurua, Nature Communications, 2012, **3**, 825.

38 J. A. Scholl, A. García-Etxarri, A. L. Koh and J. A. Dionne, Nano Letters, 2013, **13**, 564–569.

39 M. Krüger, M. Schenk, P. Hommelhoff, G. Wachter, C. Lemell and J. Burgdörfer, New Journal of Physics, 2012, **14**, 085019.

40 O. Gunnarsson and B. Lundqvist, Physical Review B, 1976, **13**, 4274.

41 K. Burke, J. Werschnik and E. Gross, The Journal of Chemical Physics, 2005, **123**, 062206.

42 D. Kosloff and R. Kosloff, Journal of Computational Physics, 1983, **52**, 35–53.

43 R. Kosloff, The Journal of Physical Chemistry, 1988, **92**, 2087–2100.

44 C. C. Marston and G. G. Balint-Kurti, The Journal of Chemical Physics, 1989, **91**, 3571–3576.

45 R. Kosloff, Dynamics of molecules and chemical reactions, 1996, 185–230.

46 M. D. Feit, J. A. Fleck and A. Steiger, Journal of Computational Physics, 1982, **47**, 412–433.

47 M. D. Feit and J. A. Fleck Jr, The Journal of Chemical Physics, 1983, **78**, 301–308.

48 W. Kohn and L. J. Sham, Phys. Rev., 1965, **140**, A1133–A1138.

49 P. B. Corkum, Physical Review Letters, 1993, **71**, 1994.

50 G. G. Paulus, W. Becker, W. Nicklich and H. Walther, Journal of Physics B: Atomic, Molecular and Optical Physics, 1994, **27**, L703.

51 G. Paulus, W. Becker and H. Walther, Physical Review A, 1995, **52**, 4043.

52 R. G. Forbes, Applied physics letters, 2006, **89**, 113122.